Angular dependence of K-shell ionization in ion-atom collisions

E. Morenzoni,* R. Anholt, S. Andriamonje,† and W. E. Meyerhof
Department of Physics, Stanford University, Stanford, California 94305
(Received 22 November 1983)

K-shell ionization probabilities P_K in 0.6–2-MeV $p+$Cu, $p+$Mo, and $p+$Ag and 0.92–2.56-MeV/amu O+Cu, O+Zr, O+Ag, and O+Pb collisions were measured at scattering angles θ between 9° and 125°. Large-solid-angle, plastic-scintillator detectors were used to detect scattered particles. The measured ionization probabilities were fitted to the expression $P_K(\theta)=A(1+B\cos\theta)$. Factors affecting values of B in various theories of K-shell ionization are discussed. The measured B values are compared with two models: an atomic model which approximates the electronic wave functions with atomic united-atom wave functions centered on the heavier nucleus and a molecular model which uses atomic wave functions of varying charge and center, optimized by minimizing the electronic energies. The present data agree best with the atomic model for proton collisions and the molecular model for oxygen collisions.

I. INTRODUCTION

The simplest theory of K-shell ionization in ion-atom collisions suggests that the probability P_K should be independent of the center-of-mass scattering angle for angles θ larger than about 10°.[1] Ionization occurs in collisions with impact parameters of the order of the inverse of the momentum transfer q_0 ($=E_K/\hbar v$, where E_K is the K-shell binding energy and v is the projectile velocity) which may be larger than 1000 fm. Large-angle ($\theta \gtrsim 10°$) scattering requires impact parameters b smaller than 100 fm, however, so that $P_K(\theta)$ should be constant in the relatively small b range below 100 fm.

Nevertheless, large-angle K-shell ionization-probability dependences were hypothesized,[2] which were only recently measured.[3–7] Most work emphasizes the influence of dipole transitions on the angular dependence.[3,8–12] A term in the perturbation Hamiltonian due to the recoil of the target nucleus in collisions with large scattering angles partially cancels contributions from the dipole part of the projectile-electron Coulomb potential. The implication of these effects if molecular electronic wave functions are used[11] and if approximate one-electron atomic wave functions are used[12] have also been considered. Monopole ionization probabilities also show an angular dependence, however.[8] The relative internuclear velocity decreases at the small internuclear distances where K-shell ionization occurs,[1] due to Coulomb repulsion between the projectile and target nuclei. It then becomes more difficult to excite the K electron, leading to smaller ionization probabilities. The angular dependence occurs because the ion slows down more in head-on collisions than in grazing ones.[13] Finally, while the use of relativistic electronic wave functions gives increased calculated ionization cross sections and probabilities at all impact parameters,[14,15] the angular anisotropy is also affected because the relative contributions from monopole and dipole transitions varies with Z when relativistic wave functions are used.

Because of all these factors, measurements of K-shell ionization at large scattering angles may provide more sensitive tests of ionization theories than cross-section or large-impact-parameter probability measurements. An additional motivation for these studies are recent measurements of compound nucleus x rays[16,17] or K-shell ionization near nuclear scattering resonances,[18,19] which are also made at large scattering angles. Intepretation of these results requires an understanding of the various factors which can affect ionization at large scattering angles.[20]

Accurate measurements at small impact parameters are difficult because the ionization probabilities are very small and few particles scatter to large angles. Convenient true x-ray–particle coincidence counting rates are usually accompanied by large random-coincidence counting rates,[3] necessitating long runs at lower count rates. The only way to improve the accuracy of such measurements is to use very large solid-angle x-ray and particle detectors. To this end we constructed eight plastic-scintillator particle detectors subtending solid angles as large as 0.8 sr that allowed us to measure x-ray–particle coincidences at eight different scattering angles simultaneously. With these detectors, probabilities with typical statistical accuracies of ±5% could be measured in less than 12 h with better than a one-to-one true- to accident-coincidence counting ratio.

Section II of this paper describes the particle detector and the coincidence counting method and presents the results. Section III discusses theoretical effects on K-shell ionization at large scattering angles and describes the particular atomic and molecular theories with which the data are compared in Sec. IV.

II. EXPERIMENT

X-ray–particle coincidences were measured using plastic-scintillator detectors for scattered particles and a NaI detector subtending 2.4 sr for x rays. Figure 1 shows a schematic diagram of the experimental setup. A beam of protons from the Stanford 3-MV Van de Graaff accelerator or oxygen from the Tandem Van de Graaff accelerator bombarded ~100-μg/cm^2-thick Cu, Mo, Zr, Ag,

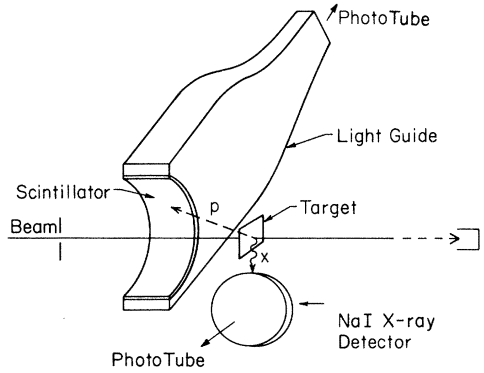

FIG. 1. Sketch of experimental arrangement described in text. Only one particle detector is shown. Five more detectors similar to that shown are arranged in parallel along the beam axis. The 9° and 29° detectors are circular detectors viewed by photomultiplier tubes in the forward direction.

TABLE I. Detector angles.

Detector	$\langle\theta\rangle$[a]	$\Delta\theta$[a]	$\Delta\phi$[a]
1	125	20	180
2	107	15	180
3	90	20	90
4	72	15	60
5	60	11	66
6	39	6	22
7	29	$\Delta\Omega=9.65\times10^{-3}$ sr[b]	
8	9	$\Delta\Omega=1.24\times10^{-4}$ sr[b]	

[a]In degrees.
[b]Circular detector.

or Pb targets positioned at 45° to the beam direction. With the exception of the 9° and 29° detectors, each particle detector consists of a 1.5-mm thick aluminized plastic-scintillator ribbon curved around the beam axis in a semicircle and mounted on a lucite light pipe which brings light out of the vacuum chamber into a photomultiplier tube. Since the particle elastic scattering cross section varies rapidly with scattering angle and since there is no advantage to count small-angle coincidences at rates much larger than large-angle coincidences, various polar angle widths $\Delta\theta$ and azimuthal angle widths $\Delta\phi$ were chosen to obtain approximately identical counting rates in all detectors. Thus, while the 107° detector subtended 0.8 sr, the 9° detector subtended 1.24×10^{-4} sr. Table I lists the opening angles used in the detectors.

The electronic techniques employed are unusual and potentially useful not only in experiments with plastic-scintillator particle detectors but also with gas ionizaton counters. Basically, standard fast-slow coincidence counting techniques were employed. A computer was used to sort and write on magnetic tape the value of the x-ray energy, particle energy, and the time difference between the x-ray and particle signals for each coincidence event. Figure 2 shows the schematic electronic setup. There are

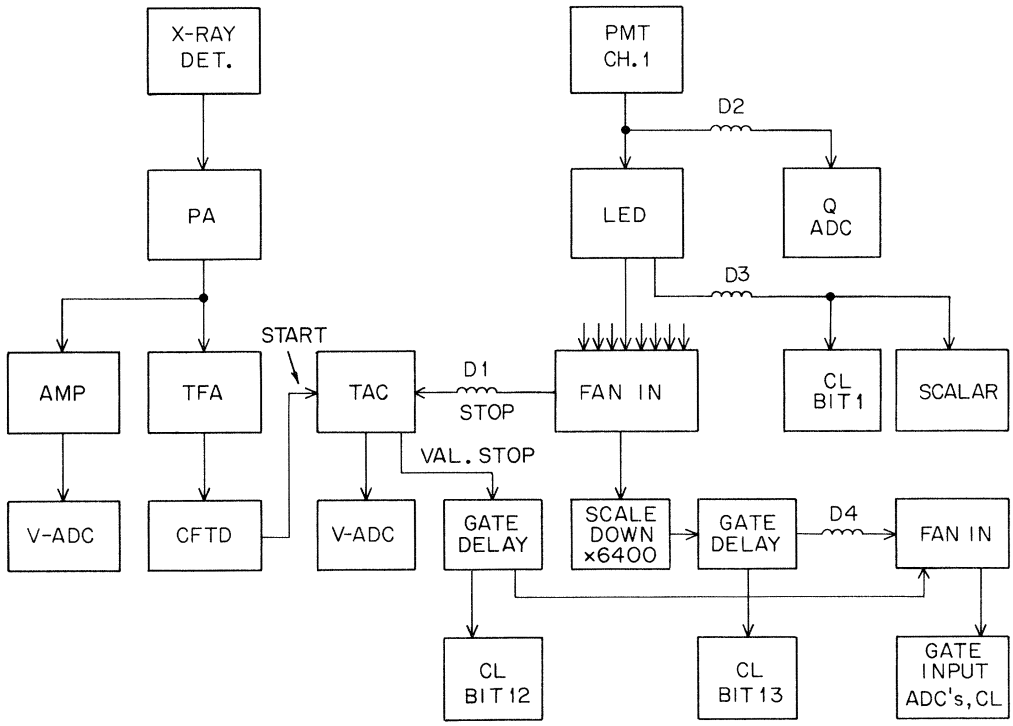

FIG. 2. Schematic electronic circuit used to measure x-ray—particle coincidences. PMT, photomultiplier tube; PA, preamplifier; AMP, amplifier; TFA, timing filter amplifier; CFTD, constant fraction timing discriminator; V-ADC, peak sensing ADC; Q-ADC, charge sensitive ADC; LED, leading-edge discriminator; CL, coincidence latch generating the event descriptor word; TAC, time-to-pulse height convertor. Only one particle channel is shown and many logic modules have been omitted. Delay $D1$ ($\simeq$190 ns) adjusts the true-coincidence peak to the middle of the TAC scale. $D2$ ($\simeq$300 ns) and $D3$ ($\simeq$320 ns) synchronize the PMT anode pulse and logic pulse at the Q-ADC and CL with the gate pulse originating from the TAC valid stop. $D4$ (80 ns) synchronizes the particle singles sample gate pulse with the true-coincidence gate pulse.

three noteworthy features. First, to measure the particle energy we used a charge-sensitive analog-to-digital convertor (Q-ADC) connected directly to the anode of the photomultiplier tube. In addition to handling very high counting rates, this saves the cost of a preamplifier to integrate the anode pulse and an amplifier to shape it for a peak sensing ADC, but 58 m of coaxial delay cable ($D2$ in Fig. 2) are needed to delay the pulse until a signal arrives from the time-to-pulse height convertor reporting an x-ray—particle coincidence. A separate Q-ADC was used for each detector. Second, to normalize the ionization probability we simultaneously sampled the particle spectrum. For every (typically) 6400 particles counted, one event is read into the computer, independent of whether there is an x-ray coincidence or not. Third, to identify the events in the computer, we also generated an event descriptor word. If the event was a coincidence, say, between channel 5 particles and x rays, bits 5 and 12 of this event descriptor word would be set equal to one; if the event was a particle singles event when, say, detector 6 fired, the descriptor word would have bits 6 and 13 set. Fast 30-nsec-wide gating was used to generate this word so that even though the total particle counting rate could exceed 10^5 Hz, events where two particle dectectors sent signals to the event descriptor word within the gating period were rare and were discarded. Owing to the small ionization probability and particle sampling rate, events where singles (bit 12) and coincidences (bit 13) appeared simultaneously were also rare.

To obtain the ionization probability for a given particle detector n (or angle θ_n), we put a gate on the true-coincidence peak of the time-difference spectrum (later subtracting the contribution from random coincidences), a gate on the particle energy for detector n, and a gate on bits 12 and n, and projected the x-ray spectrum. The K x-ray line was then integrated to obtain the number of coincident K x rays. The ionization probability is proportional to this number divided by the number of particles falling within the same particle energy window and having bits 13 and n set, and by the sampling factor (6400 in this example). The time spectrum generally had a <30-nsec wide true-coincidence peak with a flat random-coincidence background over the range of 200 nsec, giving about a one-to-one total true- to random-coincidence ratio.

The relative x-ray detector efficiency was determined by measuring x-ray cross sections for 1.5-MeV protons relative to Rutherford elastic scattering into a surface-barrier particle detector of known solid angle. Tabulated[21] x-ray cross sections were compared with these measured ones to obtain the x-ray detector efficiency. However, since a different geometrical arrangement was used in the calibration measurements, the absolute detector efficiency was not determined, so the absolute ionization probabilities were obtained by normalization to the 1-MeV $p+$Ag, results of Chemin *et al.*[5]

Figure 3 shows the angular dependence of target K-shell ionization in 1-MeV $p+$Mo and 0.92-MeV/amu O + Pb collisions. The vertical error bars in this figure represent the statistical uncertainty in each measurement. The horizontal bars indicate the range of polar angles θ subtended by each detector (see Table I). Within the statistical uncertainty of this experiment most probabilities were found to be consistent with the relation[3]

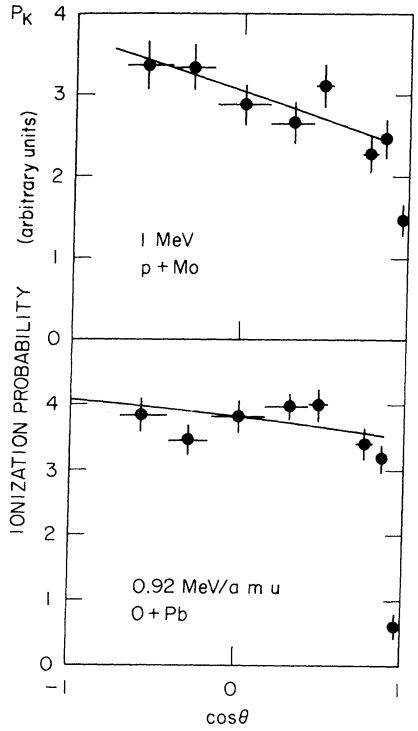

FIG. 3. Relative ionization probabilities in 1-MeV $p+$Mo and 0.92 MeV/amu ^{16}O + Pb collisions. The lines are the least-squares fits to Eq. (1).

$$P(\theta)=A(1+B\cos\theta)\ . \tag{1}$$

The constants A and B were found by linear least-squares fitting and are listed in Table II. [The 9° point was usually omitted from this fit, since it lies on the part of the $P(b)$ curve falling off as $\sim\exp(-2qb)$.[1]] Although a universal dependence of B on the parameter $\xi_K=2v/\theta_K v_K$ ($\theta_K=E_{Ku}/Z_K^2$ Ry, $Z_K=Z_1+Z_2-0.3$, $E_{Ku}=$ the united-atom $1s$ binding energy, and $v_K=Z_K$ a.u.) is not always valid (see Sec. III), we compare our proton B values with the $p+$Cu results of Andersen *et al.*[13] in Fig. 4. [Although other measurements of $P_K(\theta)$ have been made,[4–8] few report fitted B values, hence they have not been included in this figure.] The B values are basically in agreement with Andersen *et al.*,[3] but are obtained with higher precision.

Finally, we discuss the limitations of plastic-scintillation detectors for protons and heavy ions. Although a plastic scintillator (Nuclear Enterprises 102) produces sufficient light for the ions used in this experiment, the detectors have inadequate resolution even under the best of circumstances to separate elastically and inelastically scattered particles or to separate target elastic scattering from impurity carbon and oxygen elastic scattering. Therefore, our targets, with the exception of Pb, were chosen to have little carbon and oxgyen content. This was verified in separate Rutherford back-scattering measurements using surface-barrier particle detectors. In-

TABLE II. Measured A and B values in Eq. (1).

Beam	Energy MeV/amu	Target	ξ_K[a]	A[b]	B
p	0.60	Cu	0.466	1.14±0.28(−4)	−0.207±0.066
p	0.60	Mo	0.297	7.6 ±1.9(−6)	−0.435±0.037
p	1.00	Mo	0.384	4.4 ±1.1(−6)	−0.221±0.062
p	2.00	Mo	0.543	2.11±0.53(−4)	−0.084±0.055
p	1.00	Ag	0.335	1.75±0.44(−5)	−0.371±0.086
p	2.00	Ag	0.474	1.18±0.30(−4)	−0.127±0.067
^{16}O	1.93	Cu	0.644	2.16±0.54(−2)	+0.094±0.085
^{16}O	0.925	Zr	0.322	6.78±1.7(−4)	−0.055±0.106
^{16}O	2.56	Zr	0.536	8.75±2.19(−4)	−0.001±0.079
^{16}O	0.925	Ag	0.271	3.14±0.78(−4)	+0.026±0.043
^{16}O	1.64	Ag	0.361	1.87±0.47(−3)	−0.054±0.044
^{16}O	1.93	Pb	0.208		−0.062±0.055

[a]Reduced velocity calculated using the united-atom charge as explained in text.
[b]Normalized to data of Chemin *et al.* (Ref. 5).

elastic nuclear scattering prevented measurements at energies exceeding the nuclear Coulomb barrier. In retrospect, the light collection scheme used in these measurements was inefficient, so that the particle spectra at the largest angles had far worse resolution than that theoretically obtainable. To separate noise from the real particle pulses we experimented with several increasingly narrow particle-energy windows, extending downward from the highest point in the spectrum. The possible presence of noise at lower particle energy reduces the inferred ionizaton probability. A correct window occurs at the point where further narrowing would not alter the ionization probability.

III. THEORY

The excitation of K-shell electrons into the continuum is caused by the Coulomb interaction between the projectile nucleus of charge Z_p and electron. The ionization probability can be calculated with the semiclassical approximation using[1]

$$P_K(\theta)=\int_0^\infty d\epsilon \sum_{l,m} |a_{lm}(\epsilon,b,v)|^2 , \tag{2}$$

where ϵ, l, and m are the continuum-state energy and angular momentum quantum numbers, b is the impact parameter classically related to the scattering angle, the ionization amplitude is given by[1]

$$a_{lm}=-\frac{i}{\hbar}\int_{-\infty}^{\infty} dt \left\langle \epsilon lm \left| \frac{Z_p e^2}{|\vec{R}-\vec{r}|} \right| 1s \right\rangle e^{i\omega t} , \tag{3}$$

$\hbar\omega=E_K+\epsilon$, $\vec{R}(t)$ is the internuclear coordinate, and $\vec{r}$ is the electron-target nucleus coordinate. If the time integral in Eq. (3) is done along a straight-line projectile trajectory, one obtains[1]

$$dP_K(b)/d\epsilon \sim \exp(-2qb) , \tag{4}$$

where here $q^{-1}=\hbar v/(E_K+\epsilon)$ varied between 200 and 1000 fm. Scattering to angles greater than 30° requires impact parameters[6] smaller than $\sim 2d$, where d is the distance of closest approach in a head-on collision. Since in the collisions we studied the value of $2q2d$ with $\epsilon=0$ was smaller than unity, the straight-line theory suggests that $P_K(\theta)$ should be approximately θ independent.

Large-angle dependences are obtained if the time integral in Eq. (3) is done along a Coulomb trajectory. For monopole transitions ($l=0$ and $m=0$), $P_{K0}(b)$ decreases with smaller b (larger scattering angle) as shown in Fig. 5 for 0.7-MeV p + Ag collisions (reproduced from Ref. 8). This behavior, seen in many calculations,[8,13,22,23] is physically interpreted[13] as due to the reduced collision velocity at small internuclear distances and impact parameters as a consequence of the Coulomb deflection of the projectile. Reduction of the collision velocity in the region where excitation occurs[1] leads to smaller ionization probabilities.

The mathematical equation needed to express the monopole ionization probability at large scattering angles is not known and may be considerably more complicated than Eq. (1). Since the probability is smallest at the larg-

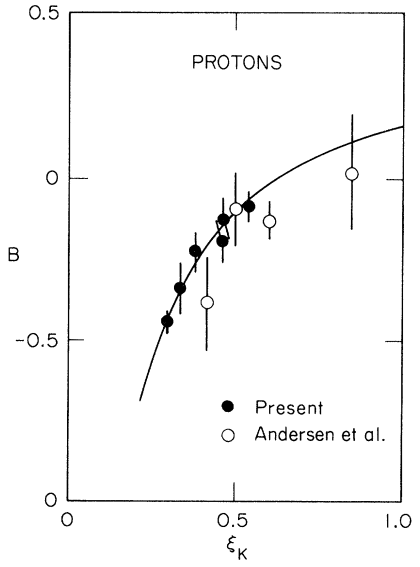

FIG. 4. B values from Table II plotted vs the united-atom reduced velocity parameter ξ_K compared with values of Andersen *et al.* (Ref. 3). The solid line is drawn to guide the eye.

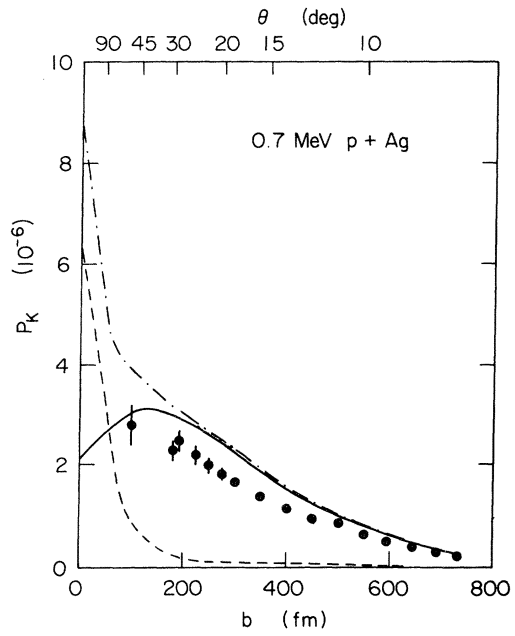

FIG. 5. Ionization probabilities in 0.7-MeV p + Ag collisions as a function of impact parameter b and scattering angle θ, taken from Ref. 8. The monopole excitation probability (solid line) which decreases at large scattering angles, the dipole excitation probability (dashed line) which increases with increasing scattering angle and the total ionization probability (chain curve) are shown. Data from Lund *et al.* (Ref. 24).

est scattering angle, positive B values for monopole excitation are implied.

For dipole transitions, negative B values are generally obtained at low collision velocities, as indicated in Fig. 5. When integrated along a Coulomb trajectory, Eqs. (2) and (3) give a dipole transition probability that varies as[3,20]

$$P_{K1}(\theta)=A_1(1-\cos\theta)\ , \tag{5}$$

implying a B value of -1. However, a part of the perturbation Hamiltonian omitted from Eq. (3) is the recoil potential.[3,8–11] In the atomic model the electronic wave function centered on the target nucleus receives a significant impulse from the projectile nucleus in collisions with large scattering angles. The recoil potential is proportional to the product of this impulse $\ddot{\vec{R}}(t)$ and the electron coordinate $\vec{r}$, which allows electron dipole excitation to the continuum. The probability obtained from this contribution alone also varies as $(1-\cos\theta)$. However, the contribution to the ionization amplitude from the recoil Hamiltonian must be added coherently to that from the Coulomb part. The two may even cancel one another for some projectile-target combinations. It has been shown that, if both contributions are included, A_1 varies as[12]

$$A_1=C\left[\frac{Z_1}{M_1}-\frac{Z_2}{M_2}\right]^2\ , \tag{6}$$

where M_1 is the projectile mass number, M_2 is the target mass number, and C is a constant. Combining Eqs. (5) and (6) with the monopole ionization probability which we assume to vary as $A_0(1+B_0\cos\theta)$, we see that the total

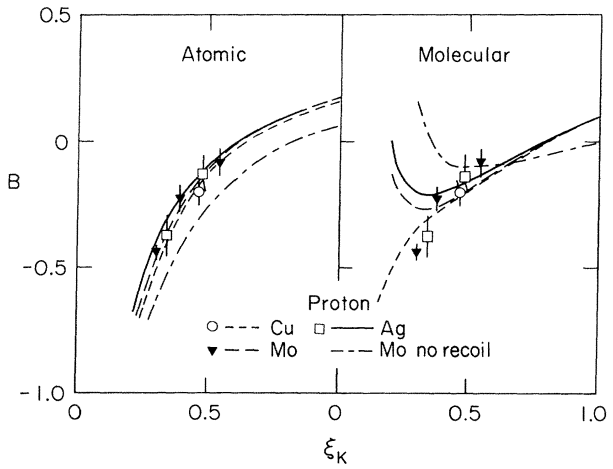

FIG. 6. Calculated and measured B values for p + Cu, p + Mo, and p + Ag collisions. The chain curve gives the B values for p + Mo calculated assuming zero recoil contributions.

probability is

$$P_K=A_0(1+B_0\cos\theta)+A_1(1-\cos\theta)$$
$$=A(1+B\cos\theta)\ , \tag{7}$$

where $A=A_0+A_1$ and $B=[A_0B_0-C(Z_1/M_1-Z_2/M_2)^2]/(A_0+A_1)$. Assuming that $Z_2/M_2\simeq\frac{1}{2}$, we see that for protons $(Z_1/M_1=1)$ B is more negative than for ^{16}O ions where $Z_1/M_1\simeq Z_2/M_2$. This trend is clearly seen in our data (Figs. 6 and 7).

In low-velocity collisions the K electrons can partially adjust their motion to the presence of the projectile nucleus, so that in principle a diatomic molecular wave function around the projectile and target nuclei is more appropriate than an atomic wave function centered on the heavier partner. The molecular effect most often discussed[15,25] is the increased binding of the $1s$ electron, which makes it more difficult to excite the electron and results in smaller ionization probabilities. The use of molecular wave functions also affects the recoil considera-

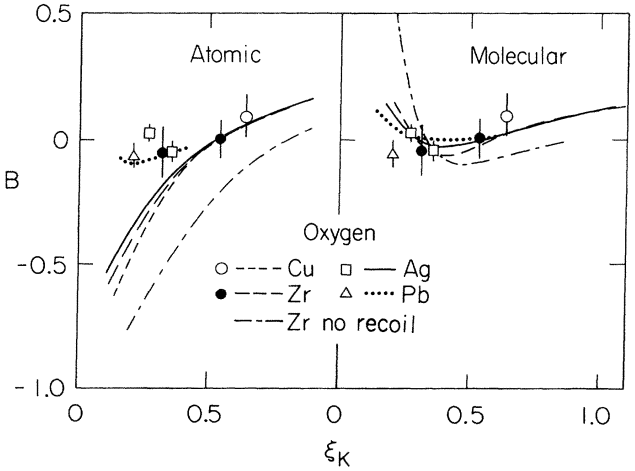

FIG. 7. Calculated and measured B values for O + Cu, Zr, Ag, and Pb collisions. The chain curve shows the B values calculated assuming no recoil contribution.

tions because the molecular wave functions are centered on the center of charge and not on the heavier nucleus and the recoil potential depends on the wave-function reference frame. Also, the perturbation Hamiltonian is different; the interaction is not just the projectile-electron Coulomb potential but a $\hbar\partial/\partial t$ operator.[26]

Two other wave-function effects can also affect the magnitude of B. Relativistic electronic wave functions must be used to obtain accurate cross sections and ionization probabilities at low velocities.[14,15] In our calculations employing one-electron Dirac wave functions, the contribution to the ionization probability from dipole transitions decreases relative to monopole transitions with increasing atomic number for a given value of ξ_K. This causes a Z_2 dependence of B on ξ_K, even if the mass ratios Z_2/M_2 were independent of Z_2. Although one-electron wave functions have consistently given accurate ionization cross sections when screening factors are included,[25] they are probably inadequate for calculating B values. Expression (6) is obtained only if one has correct many-electron wave functions.[12] An *ad hoc* modification of the recoil potential has been suggested so that results similar to those in Eq. (6) are obtained when hydrogenic wave functions are used.[12] The validity of this modification has not been tested against many-electron wave functions, however.

In this paper, we compare our data with two different models: an "atomic" model, based on the ideas of Andersen *et al.*[27] and a "molecular" model described by Anholt.[11] Both models account approximately for binding and relativistic effects. In the atomic model we use united-atom (UA) Dirac one-electron $1s$ and continuum wave functions centered on the heavier nucleus. The wave function center is the same as in the unmodified atomic theories; hence, the dipole transition considerations will be identical to those discussed above, Eqs. (6) and (7).

In the molecular model we use a wave function of varying charge $Z(R)$ centered at a distance $\vec{\mathrm{R}}h(R)$ from the heavier nucleus. This modifies the Coulomb potential which becomes[11]

$$V_M = -\frac{Z_1 e^2}{|\vec{r}-\vec{\mathrm{R}}(1-h)|} - \frac{Z_2 e^2}{|\vec{r}-h\vec{\mathrm{R}}|} \tag{8}$$

and the recoil potential which becomes

$$H_R = -\frac{\partial^2[(h-g)\vec{\mathrm{R}}]}{\partial t^2}\cdot\vec{r}\,, \tag{9}$$

where $g \equiv M_1(M_1+M_2)^{-1}$. The quantities $Z(R)$ and $h(R)$ are obtained by variationally minimizing the molecular $1s$ electronic energy.[28] The quantities have expected properties. At $R=0$, $Z(R)$ is the UA charge and at $R=\infty$, it is the higher-Z charge. At $R=0$, $h(R)$ is equal to $Z_1(Z_1+Z_2)^{-1}$ which means that the wave function is centered on the center of charge of the two nuclei and at $R=\infty$, $h(R)$ is zero, so that the wave function correlates to the heavier collision partner.

Anholt[11] has shown that qualitatively the two theories give similar results, for the dipole transitions. At small internuclear distances, where $h \simeq Z_1(Z_1+Z_2)^{-1}$, the dipole part of V_M can be expanded as

$$V_{M1} \sim -\frac{R}{r^2}\hat{R}\cdot\hat{r}[Z_1(1-h)-Z_2 h]\,, \tag{10}$$

which is identically zero; the dipole part of the Coulomb potential between the target nucleus and electron cancels that between the projectile nucleus and electron. Therefore, only the recoil Hamiltonian will contribute to A_1 at large scattering angles. Hence, in the molecular theory one finds, approximately,

$$A_1 \sim (g-h)^2 \sim C_M\left[\frac{Z_1}{Z_1+Z_2}-\frac{M_1}{M_1+M_2}\right]^2, \tag{11}$$

where C_M is a constant. As long as $Z_1 \ll Z_2$ and $M_1 \ll M_2$ this expansion gives predictions similar to the atomic model, Eq. (6).

Both theories make calculations of ionization probabilities by integrating along Coulomb trajectories. Also, one-electron Dirac wave functions are used without any *ad hoc* modifications to the recoil Hamiltonian. More details can be found in Ref. 11.

IV. RESULTS

To compare our results with theory, in Figs. 6 and 7 we plot the experimental B values (Table II) against the parameter ξ_K, where ξ_K is calculated with united-atom number and binding energy. $B(\xi_K)$ is not expected to be independent of the atomic number Z_2; therefore theoretical curves for different target atomic charges are displayed. One can observe an interplay between the positive monopole contributions to B which increase with lower ξ_K and the dipole contributions which make B more negative with lower ξ_K. In the atomic model, since Z_2/M_2 in Eq. (6) decreases with higher Z_2, one expects the relative dipole contribution to become larger with Z_2, but the effect is reduced because at higher Z_2 the use of relativistic wave functions decreases the dipole relative to the monopole ionization probability. In the molecular calculations, the monopole contributions overwhelm the dipole contributions completely at small ξ_K, so that the B curves for $Z_2 > 30$ turn up below $\xi_K = 0.3$.

If one turns off the recoil contribution, B becomes more negative in the atomic calculations and more positive in the molecular ones at small ξ_K. Since in the molecular calculations the contribution from the dipole part of the Coulomb potential is near zero, turning off the recoil potential leaves only the monopole probability which has high positive B values for small ξ_K. In the atomic calculations, by turning off the recoil contribution one is essentially setting Z_2/M_2 in Eq. (6) to zero, leading to larger dipole contributions to B. The data definitely show the necessity of including the recoil contribution. In either model, one obtains smaller B values for oxygen ions $Z_1/M_1 = \frac{1}{2}$ than for protons $Z_1/M_1 = 1$, indicating the importance of the dipole transitions.

The data agree best with the atomic theory for protons and with the molecular theory for oxygen ions as shown in Fig. 8. For protons the atomic calculations give a nearly Z_2-independent $B(\xi_K)$ value, which agrees well with

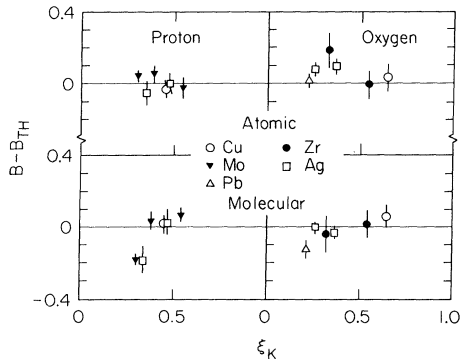

FIG. 8. Differences between measured and calculated B values.

the data, over this limited range of Z_2 values. The p + Mo and p + Ag points at the lowest velocities clearly disagree with the molecular calculations. For oxygen ions the two lowest-velocity Ag and the lowest-velocity Zr data points disagree with the atomic calculations, but the O + Pb point disagrees with molecular ones.

Figures 9 and 10 compare the measured A values [$P_K(90°)$] with the atomic and molecular calculations. We emphasize that we did not measure A absolutely but normalized our probabilities to those of Chemin *et al.*[5] For protons, there is little difference between the two theories; both account for the binding effect by using UA

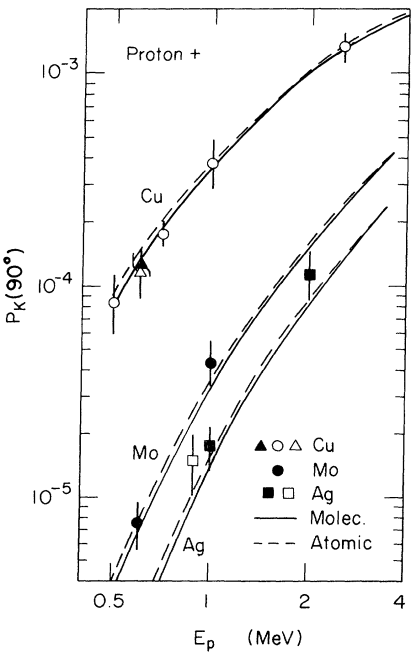

FIG. 9. Ionization probability at 90° [A value in Eq. (1)] for p + Cu (▲), Mo (●), and Ag (■) for various proton energies. Solid curve, molecular theory; dashed line, atomic theory. Solid points are present work. Open circles are A values from Andersen *et al.* (Ref. 3). (No error in their value was reported, so the errors shown are typical data-point uncertainties.) Also shown are probabilities for 0.6-MeV p + Ni at $\theta=80°$ (Δ) and 0.9-MeV p + Ag at $\theta=91°$ (□) from Schmidt-Böcking *et al.* (Ref. 7) (A and B were not calculated in this work).

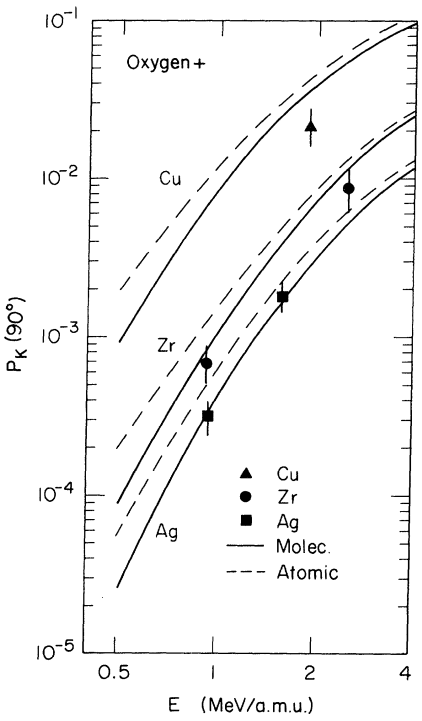

FIG. 10. Ionization probability at 90° for O + Cu, Zr, and Ag collisions. Solid curve, molecular theory; dashed curve, atomic theory.

electronic wave functions and energies in the atomic model and by varying the charge and energies in the molecular. Within the experimental uncertainties, the proton data agree with both theories. The oxygen data agree better with the molecular theory than the atomic theory, especially for Ag and Zr.

V. CONCLUSIONS

Measurements of relative ionization probabilities at large scattering angles in low-velocity ion-atom collisions can provide a sensitive test of K-shell ionization theories. This paper has summarized the expected effects on monopole and dipole ionization probabilities stemming from the use of atomic or molecular, relativistic or nonrelativistic, and one- or many-electron wave functions. Although the ionization probabilities at a fixed impact parameter for protons do not depend sensitively on the details of the model used, the calculated B values can differ very much. Also, one can measure the relative probabilities to obtain B values more accurately than the absolute probabilities, which depend sensitively on calibration uncertainties.

Our data is compared with an atomic and molecular model of K-shell ionization. It should be emphasized that both of these theories account approximately for the major molecular effect: the increased binding of the $1s$ electron. The distinction between molecular and atomic here refers mainly to the assumed reference frame of the electronic wave functions. The $1s$ wave function is centered on the higher-Z partner in the atomic theory and near the center of charge at small internuclear distances in the

molecular one. Overall, the data appears to favor the present atomic model for proton-induced collisions and the molecular model for oxygen-induced collisions. The exceptional point is for O + Pb where the atomic model is favored. In either model the data clearly indicate the importance of the recoil contribution to K-shell ionization.

Open questions remain which must be addressed theoretically. The mathematical form expressing the monopole ionization probability has only approximately an $A_0(1+B_0\cos\theta)$ dependence. The exact form is not known, although our total ionization-probability calculations generally give an approximately linear dependence on $\cos\theta$ for the ξ_K values shown. The effects stemming from the use of many-electron wave functions, though discussed, have not been addressed in this work. Although alterations of the dipole recoil-potential cancellation in the atomic theories are expected, they have not been included here. At very low velocities, where the energy lost exciting the K electron becomes comparable to the total center-of-mass energy, further modifications of the K-shell ionizaton probability are expected, which only quantum-mechanical calculations can address. How this affects the relative ionization probabilities at large scattering angles is not known.

ACKNOWLEDGMENTS

Some of the experimental techniques used in these measurements were learned from D. L. Clark, J. Napolitano, and A. Litke. We thank J. Molitoris and O. K. Baker for assisting in data taking. This work was supported in part by the National Science Foundation Grant No. PHY-80-15348. One of us (E.M.) was a recipient of a fellowship from the Swiss National Funds; another (S.A.) was a recipient of a North Atlantic Treaty Organization fellowship.

---

*Present address: Swiss Federal Institute of Technology, CH-8093 Zurich, Switzerland.

†Present address: Centre d'Etudes Nucléaires de Bordeaux-Gradignan, F-33170 Gradignan, France.

[1]J. Bang and J. M. Hansteen, K. Dan. Vidensk. Selsk. Mat. Fys. Medd. 31, 13 (1959).

[2]G. Ciocchetti and A. Molinari, Nuovo Cimento B 40, 69 (1965).

[3]J. U. Andersen, L. Kocbach, E. Laegsgaard, M. Lund, C. D. Moak, J. Phys. B 9, 3247 (1976).

[4]J. F. Chemin, S. Andriamonje, J. Roturier, B. Saboya, R. Gayet, and A. Salin, Phys. Lett. 67A, 116 (1978).

[5]J. F. Chemin, S. Andriamonje, S. Denagbe, J. Roturier, B. Saboya, and J. P. Thibaud, Phys. Rev. A 15, 1851 (1977).

[6]W. Duinker and J. van Eck, J. Phys. B 14, 4825 (1981).

[7]H. Schmidt-Böcking, K. E. Stiebing, W. Schadt, N. Lochter, G. Gruber, S. Kelbch, K. Bethge, R. Schuch, I. Tserruya, Nucl. Instrum. Methods 192, 71 (1982).

[8]P. A. Amundsen, J. Phys. B 11, 3197 (1978).

[9]D. H. Jakubassa and P. A. Amundsen, J. Phys. B 12, L725 (1979).

[10]F. Rösel, D. Trautmann, and G. Bauer, Nucl. Instrum. Methods 192, 43 (1982).

[11]R. Anholt, Z. Phys. A 295, 201 (1978).

[12]R. Anholt, Phys. Lett. 84A, 321 (1978).

[13]P. A. Amundsen, J. Phys. B 11, L737 (1978).

[14]P. A. Amundsen, L. Kocbach, and J. M. Hansteen, J. Phys. B 9, L023 (1976).

[15]R. Anholt and W. E. Meyerhof, Phys. Rev. A 16, 190 (1977).

[16]J. F. Chemin, S. Andriamonje, J. Roturier, B. Saboya, J. P. Thibaud, S. Joly, S. Plattard, J. Uzureau, H. Laurent, J.-M. Maison, and J. P. Shapira, Nucl. Phys. A331, 407 (1979).

[17]S. Röhl, S. Hoppenau, and M. Dost, Phys. Rev. Lett. 43, 1300 (1979).

[18]J. S. Blair, P. Dyer, K. Snover, and T. A. Trainor, Phys. Rev. Lett. 41, 1712 (1978).

[19]J. F. Chemin, R. Anholt, Ch. Stoller, W. E. Meyerhof, and P. A. Amundsen, Phys. Rev. A 24, 1218 (1981).

[20]J. S. Blair and R. Anholt, Phys. Rev. A 25, 907 (1982).

[21]R. K. Gardner and T. J. Gray, At. Data and Nucl. Data Tables 21, 515 (1978).

[22]P. A. Amundsen, J. Phys. B 10, 2177 (1977).

[23]L. Kocbach, Phys. Norv. 8, 187 (1976).

[24]M. Lund, Ph.D. thesis, University of Aarhus, 1974.

[25]G. Basbas, W. Brandt, and R. Laubert, Phys. Rev. A 7, 983 (1973).

[26]J. S. Briggs, J. Phys. B 11, L485 (1980).

[27]J. U. Andersen, E. Laegsgaard, M. Lund, and C. D. Moak, Nucl. Instrum. Methods 132, 507 (1976).

[28]D. H. Jakubassa, Z. Phys. A 285, 249 (1978).